Journal of Crohn's and Colitis, 2025, **19**(8), jjaf130
https://doi.org/10.1093/ecco-jcc/jjaf130
Advance access publication 18 July 2025
Original Article

Spatiotemporal analysis of Crohn's disease reveals PECAM2 signaling at the basis of the inflammation-to-fibrosis transition

Luca Massimino[1], Tommaso Lorenzo Parigi[2], Matteo Riva[1], Sabrina Nicolò[2], Carmela Errico[1], Salvatore Spanò[1], Sara Mino[3], Mattia Bugatti[3], Alice Frontali[4], Federico Scarfò[1], Andrea Vignali[2,4], Andrea Municchi[1], Vincenzo Villanacci[3], Luca Albarello[1,2], Maurilio Ponzoni[1,2], Virginia Solitano[2,4], Alberto Malesci[2] Vipul Jairath[5], Laurent Peyrin-Biroulet[6,7], Pierpaolo Sileri[2,4], Silvio Danese*[,1,2], Federica Ungaro*[,1]

[1]Gastroenterology and Digestive Endoscopy Department, IRCCS Ospedale San Raffaele, Milan, Italy
[2]Faculty of Medicine, Università Vita-Salute San Raffaele, Milan, Italy
[3]Institute of Pathology, ASST Spedali Civili and University of Brescia, Brescia, Italy
[4]Department of Colorectal Surgery, IRCCS San Raffaele, Milan, Italy
[5]Department of Medicine, Division of Gastroenterology, Western University, London, Ontario, Canada
[6]Inserm NGERE, University of Lorraine, Nancy, France
[7]Department of Hepato-Gastroenterology, University Hospital Centre Nancy, Nancy, France

*Corresponding author: Federica Ungaro, IRCCS Ospedale San Raffaele, Gastroenterology and Digestive Endoscopy Department, via Olgettina 60, 20132, Milan, Italy (ungaro.federica@hsr.it) and Silvio Danese, Gastroenterology and Digestive Endoscopy Department, via Olgettina 60, 20132, Milan, Italy (danese.silvio@hsr.it).

Author Contributions: Luca Massimino, Tommaso Lorenzo Parigi, Matteo Riva, and Sabrina Nicolò equally contributed to the work.

Abstract

Background and Aims: Crohn's disease (CD) is a chronic inflammatory disease of the bowel, often complicated by fibrotic strictures, for which medical treatment is lacking, and surgery is commonly required. The mechanisms underlying the progression from chronic inflammation to fibrosis are not yet defined. We aim to unravel CD pathogenesis using a cutting-edge computational pipeline combining several available tools.

Methods: Spatial transcriptomics was performed on 13 surgical specimens, including inflamed and fibrotic CD tissues and healthy controls. The resulting spatial data were integrated with single-cell RNA sequencing to trace the cellular and molecular transitions from healthy intestine to fibrotic tissue. Ligand–receptor interaction and pseudotime analyses were employed to infer dynamic cell–cell communication networks and lineage trajectories. Key computational findings were validated through immunostaining in an independent cohort of CD patients. Finally, the therapeutic relevance of the identified target was evaluated in a TNBS-induced chronic colitis mouse model upon CD38 inhibitor administration.

Results: We demonstrated that intestinal cytoarchitecture was rearranged while chronic inflammation progressed. CD-associated fibrosis evolved within the mesenchymal compartment, driven by PECAM2 signaling through the PECAM1–CD38 interaction. In parallel, ApoA signaling, particularly the APOA1–ABCA interaction, emerged as relevant for maintaining epithelial and stromal homeostasis, while its downregulation was associated with fibrosis development. Moreover, inhibition of CD38 signaling effectively reduced colitis symptoms and colon thickening in the experimental TNBS-induced model of chronic inflammation.

Conclusions: Our results provide insights into CD38-driven fibrosis and indicate that blockade of PECAM2 signaling could reduce the development of strictures in patients with CD, potentially offering a new treatment target.

Key words: chronic inflammation; spatial transcriptomics; fibrosis; Crohn's disease

Graphical abstract

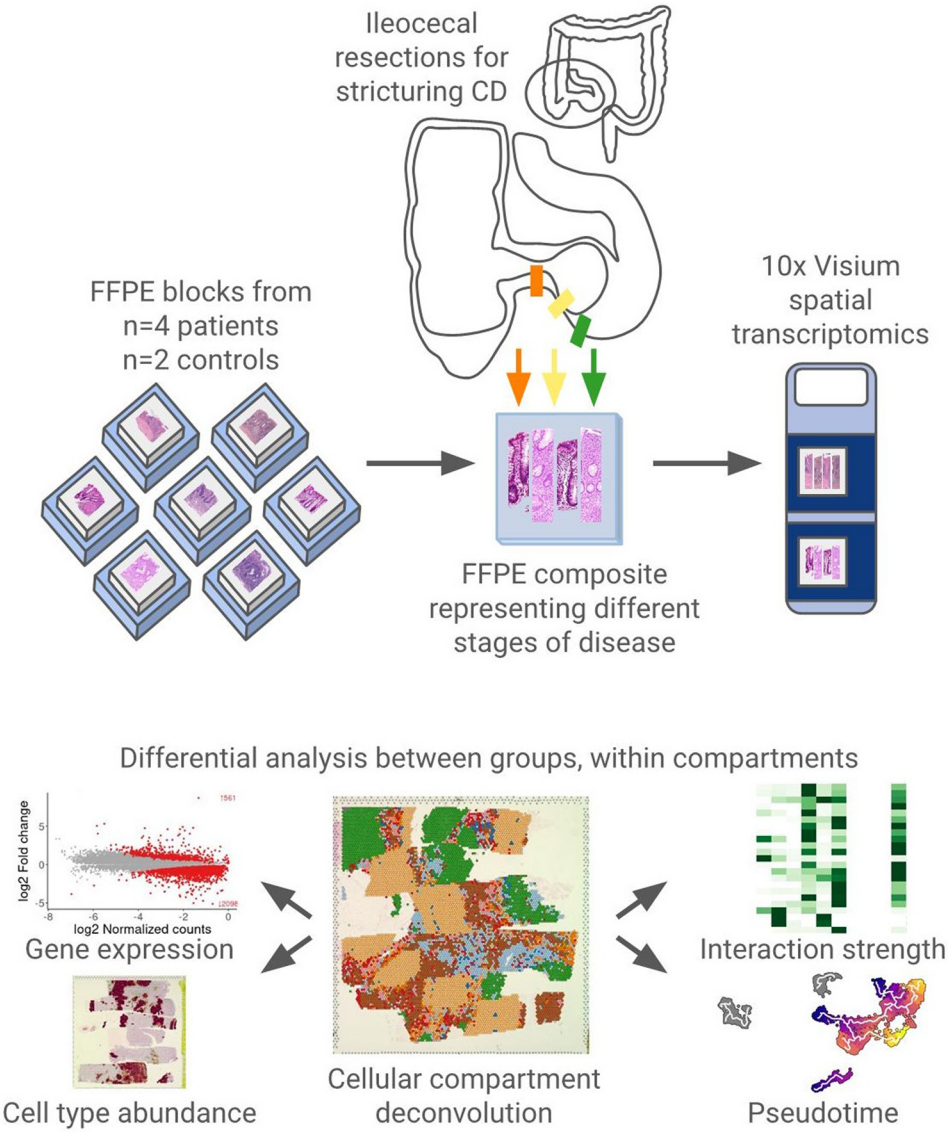

1. Introduction

Crohn's disease (CD) is a chronic inflammatory disorder with a complex and multifaceted etiology and pathogenesis, presenting striking asymmetries in location and behavior.[1] CD can affect any segment of the gastrointestinal tract from the mouth to the anus, but it is most commonly localized in the terminal ileum and/or in the colon.

Inflammation in CD involves all the layers of the gut wall from the mucosa to the serosa. This transmural pattern of disease extension is at the basis of intestinal tract stricturing, one of the most common complications of CD.

Strictures result from the accumulation of fibrosis in the lamina propria and hypertrophy of the muscularis propria.[2] Strictures occur in more than 50% of patients, most commonly in the terminal ileum rather than the colon,[2] and the only treatment options are invasive, such as surgery or balloon dilatation.

The primary cause of intestinal fibrostenosis is believed to be the continuous tissue injury occurring in chronic inflammation.[3] Despite this, the mechanisms underlying fibrotic complications in CD remain largely unclear, and specific treatment and prevention measures are missing.

The intestine is a complex, multi-layered tissue composed of diverse cell types and signaling networks, making the investigation of individual factors insufficient to grasp the processes behind CD pathogenesis. A comprehensive understanding requires integrating evidence through a multi-level approach.

Next-generation sequencing (NGS) approaches have been evolving rapidly over the years, flourishing with different technologies useful for exploring and elucidating various biological and molecular mechanisms, which would otherwise be difficult to characterize.[4]

Among these, RNA-sequencing (RNA-seq) analysis has helped understand CD pathogenesis but some technological pitfalls remain. Although bulk and single-cell RNA-seq experiments helped to identify new processes or hypotheses,[5–8] they did not fully resolve the physiological and pathological intestinal map. The advent of spatial transcriptomics (ST) has overcome this limitation by coupling transcriptomic profiles with

cellular spatial organization information without the need for sample dissociation.[9]

Here, for the first time in the context of CD, we sought to describe the pathogenic mechanisms of CD evolution toward intestinal fibrosis by assembling tissues from different stages of chronic inflammation and exploiting ST, along with state-of-the-art computational methodologies. Moreover, we show how decoding fibrosis mechanisms through ST helped to identify the PECAM2 signaling at the basis of the inflammation-to-fibrosis transition, whose inhibition ameliorated colitis and colon thickening in mice. Our study establishes ST as an adequate technology for discovering cellular and molecular processes and biomarkers orchestrating early disease and its progression, ultimately providing a novel outlook on CD and new potential targets for treatment.

2. Material and methods

2.1. Human sample selection and processing

Samples from surgical intestinal resections of CD strictures provide an ideal model of the fibrotic process unfolding. The two ends of the specimen are usually macroscopically non-fibrotic while, progressing toward the center of the segment, the thickening increases, reaching its maximum at the point of the stenosis (Figure S1(A)). In addition, variable degrees of inflammation can be present throughout the segment. Thus, macroscopically healthy margins are usually present at the resection site, and the affected tract is fully removed. Throughout its length, the surgical specimen displays the transition from the proximal healthy margin to the affected part (usually also inflamed), reaching the stricturing point and reverting to the healthy distal margin.

Based on this rationale, we selected surgical leftovers from patients undergoing ileocecal resection due to stricturing CD. The formalin-fixed, paraffin-embedded (FFPE) tissues were inspected by the pathologist to identify the three regions of interest per sample, representing the healthy region, an intermediate tract displaying inflammation with initial fibrotic changes, and the maximally affected areas with marked fibrosis and maximal strictures. After the intestinal regions of interest were identified, the original FFPE blocks were melted. The selected tissue slices were reassembled in two new paraffin blocks to optimize the sequencing surface. The correct orientation in the reassembled paraffin blocks was confirmed by examining hematoxylin and eosin (H&E)-stained slides adjacent to those cut for sequencing. Tissues were thus reassembled to create a specimen composite with a diameter of approximately 11 mm (Figure S1(B)) with CD-derived intestinal samples (Figure S1(C)) encompassing different areas of interest or "stages" of the process. This approach was required to obtain tissue slices accommodating into the 10× Visium Spatial Gene Expression slide from as many patients as possible and comprising different disease stages.

2.2. Immunohistochemistry

Immunohistochemistry (IHC) was performed on a set of human tissue samples affected by CD obtained from the archive of the Department of Pathology (ASST Spedali Civili di Brescia, Brescia, Italy). Tissue sections 4 µm thick were obtained from FFPE blocks. For immunohistochemical staining, endogenous peroxidase was blocked by incubation with methanol and hydrogen peroxide 0.03% for 20 min during rehydration. Immunostaining was performed using anti-CD38 (clone SPC32, 1:200, Novocastra, code no. NCL-L-CD38-290). After pre-treatment with microwaves in EDTA buffer at pH 8.00, the reaction was revealed using Novolink Polymer (Leica Microsystems), followed by diaminobenzidine (DAB; Dako, Glostrup, Denmark). Finally, the slides were counterstained with Meyer's Haematoxylin.

2.3. Spatial transcriptomics

ST sequencing was performed by AcelaBio (San Diego, CA). Raw reads were aligned to the human reference genome (GRCh38) and linked to the H&E images with Space Ranger (10× Genomics, v2.1.1). The resulting gene expression matrices were quality-checked, normalized, preprocessed, multi-dimensionally scaled, and clustered with Seurat (v5.3.0).[10] Data harmonization was performed with Harmony (v1.2.3).[11] Digital segmentation of the different slices was performed with SPATA2 (v2.0.4).[12] Stlearn (v0.4.12) was used for spatially resolved multi-dimensional scaling and clustering.[13] Deconvolution of spatial data with single-cell signatures and deconvolution of single-cell data with spatial signatures were performed with Seurat (v5.3.0)10, using the functions FindTransferAnchors() and TransferData(), and the 10× pre-built GRCh38 reference genome (https://www.10xgenomics.com/support/software/cell-ranger/downloads#reference-downloads). Pseudotime analysis was performed with Monocle 3 (v1.3.7).[14] Pathway analysis was performed with GSdensity (v0.1.3).[15] CellChat (v2.1.2) was used to analyze ligand–receptor and cell–cell communication.[16]

Regarding parameters, we primarily employed the default settings for these tools unless specific analytical requirements, such as data filtering thresholds, clustering parameters, or criteria for differential analysis, necessitated the use of non-default values.

Quality control steps and metrics, according to the 10×'s instructions, applied to the ST data included: (1) Overall Read Mapping; (2) Sequencing Saturation; (3) Q30 Bases; (4) Valid Barcodes and UMIs; and (5) Reads, UMI Counts, and Genes per Spot under Tissue.

Upon initial processing of raw sequencing data with Space Ranger, and following a comprehensive read count quality check confirming the absence of sequencing bias in whole tissue areas and clusters, the ST data demonstrated sufficient and unbiased data capture quality, thereby obviating the need for filtering of individual spatial spots based on metrics related to sequencing saturation or overall read count sufficiency.

2.4. TNBS model of colitis

Female C57BL/6 mice were maintained in our specific-pathogen-free (SPF) animal facility and used at 8 weeks of age. All experiments were performed following the guidelines established in the Principles of Laboratory Animal Care (Directive 86/609/EEC) and were approved by the Italian Ministry of Health. The procedures involving mice conformed to institutional guidelines in agreement with national and international law and were approved by the ethics committee of the IRCCS Ospedale San Raffaele. Based on our experience with animal models and according to animal welfare policy (directive 86/609/EEC), which strongly suggests the use of a limited number of animals, we estimated that two experiments with $n = 5$ mice per group would allow us to reach statistical significance.

Mice were randomized, and experimental mouse allocation and evaluation of clinical disease parameters by a dedicated lab technician were blinded.

C57BL/6N mice 7 weeks of age were divided into four experimental groups ($n = 5$): group I served as the control group receiving 45% ethanol (EtOH); group II received the vehicle (45% EtOH) along with a CD38 inhibitor; group III was induced with trinitrobenzene sulfonic acid (TNBS; Sigma-Aldrich, Italy) along with 45% EtOH; and group IV received both TNBS and the CD38 inhibitor (iCD38; EMD Millipore Corp., USA). TNBS induction involved intrarectal administration of TNBS dissolved in 45% EtOH at escalating doses weekly, doses ranging from 1 mg/0.1 ml to 2 mg/0.1 ml, while control mice received 45% EtOH alone. Mice in groups III and IV additionally received the CD38 inhibitor (15 mg/kg) intraperitoneally three times per week, starting from the fourth week of TNBS treatment. Mice were scored for the development of colitis symptoms, including stool consistency, body weight, and rectal bleeding, and the disease activity index (DAI) was calculated for each animal. At the end of the 7-week TNBS treatment period, followed by an additional 2-week evaluation phase, mice were killed using CO_2. Before this, all mice underwent an endoscopic evaluation to assess the degree of inflammation and mucosal damage as previously reported.[17]

3. Results

3.1. Intestinal layers rearrange while inflammation progresses with associated changes in molecular signatures

Samples from surgical intestinal resections of CD strictures provide an ideal model of the fibrotic process unfolding. The two ends of the specimen are usually macroscopically non-fibrotic while, progressing toward the center of the segment, the thickening increases, reaching its maximum at the point of the stenosis (Figure S1(A)). Based on this rationale, we selected surgical sections from patients undergoing ileocecal resection due to stricturing CD. Pathologists experienced in gastrointestinal diseases inspected the FFPE tissues to identify the three regions of interest per each sample representing the healthy region (referred to as control, and confirmed as having a Robarts Histological Index of activity <3 with no neutrophils in the lamina propria or epithelium), an intermediate tract displaying inflammation with only minimal fibrotic changes (L1), and the maximally affected area with marked fibrosis and maximal stricture (L2) (Figure 1(A)). Once the intestinal regions of interest were identified, FFPE tissues were reassembled to create a specimen composite (Figure S1(B)) with CD- and healthy subject-derived intestinal samples ($n = 13$ slices, 11 CD and 2 controls, Figure S1(C)). Spatial transcriptomics was then performed to map the spatial distribution of the cell compartments.

Since sequencing data came from the two different capture areas on the slide, we predicted a batch effect, which we assessed and counteracted with Harmony[11] (Figure S2(A) and (B)). A read count quality check was then performed confirming the absence of sequencing bias in whole tissue areas and clusters (Figure S2(C) and (D)).

To investigate the transmural progression of inflammation in CD,[18] we performed an unsupervised clustering through spatial distance, tissue morphology, and gene expression measurements with the Louvain community detection algorithm identifying 21 clusters defined by different transcriptomic signatures and spatially distributed across disease stages (control, L1, and L2) and tissue layers in each slice (Figure 1(B)). The pathologists annotated each cluster according to its characteristics (Figure 1(C)), finally identifying different compartments, including the epithelial, muscular, stromal, nervous, fibrotic, and inflammatory (lymphoid aggregates and granulation tissue) compartments. Within the compartments, the analysis revealed additional transcriptomic differences related to the location and inflammatory state (ie, deep/superficial; inflamed/not inflamed, Figure 1(C)).

We observed a progressive alteration of the cytoarchitecture along the different disease stages, paralleling disease aggravation from control to L1 and L2, as expected. Specifically, the healthy portion (control) displayed a well-assembled and intact epithelium, with two layers, one superficial and one deep. In

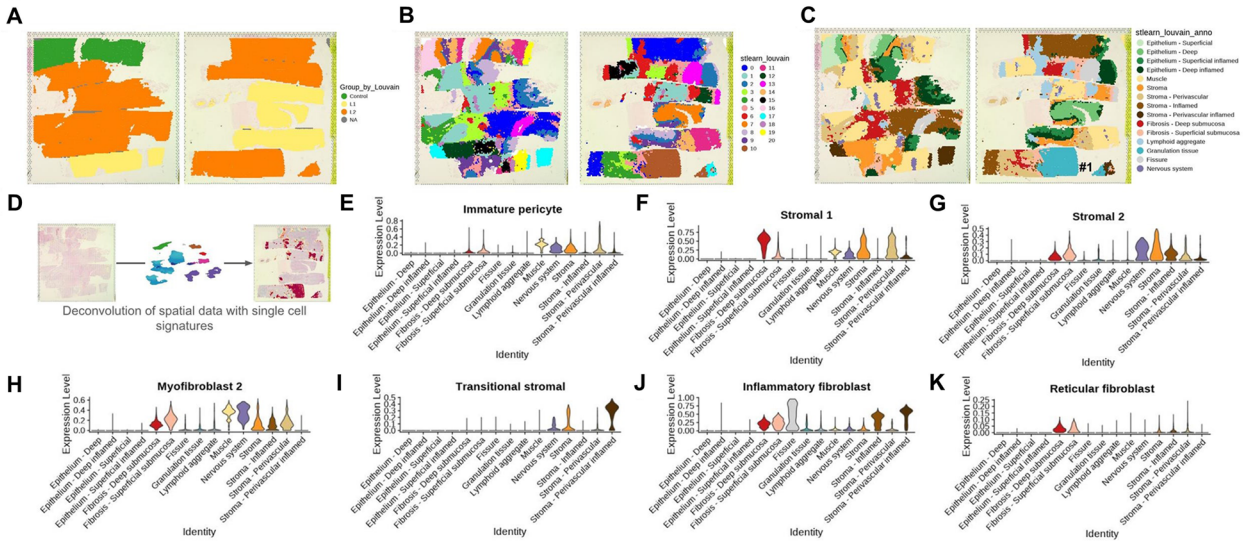

Figure 1. Intestinal mucosa compartments rearrange while inflammation progresses. (A) 10× Visium Spatial Gene Expression slides with tissue slices from control (green), L1 (yellow), and L2 (orange) areas. (B–C) Unbiased clustering by the Louvain algorithm (B) and the pathologist's cluster annotation (C) of spatial transcriptomics data in control, L1, and L2 tissue slices. (D) Schematic representation of deconvolution of spatial data with single-cell signatures. (E–K) Violin plots showing gene expression profiles related to the indicated specific cell types of the annotated cell clusters.

L1 and L2 slices, these two layers lost their physiological cytoarchitecture and transformed into inflamed epithelia (Figure 1(C)). Of note, a thin layer of deep inflamed epithelium was observed in the control. This is consistent with the specimen's nature since it came from a healthy margin of intestinal resection that might retain minimal traces of inflammation. Likewise, in the healthy tissue, the submucosa, namely the stroma and the perivascular stroma, are visible and well organized over the muscle layer, associated with enteric nervous tissue spots. In L1 and L2, this structure was altered. All stromal types became inflamed, fibrosis, distinguished in deep and superficial layers, accumulated, breaks and fissures developed on the surface, and extended lymphoid aggregates and granulation tissues appeared (Figure 1(C)).

These spatial data confirmed CD-associated rearrangement of the intestinal layers[19] in terms of localization and molecular signatures while inflammation progressed and complications developed.

3.2. Cell clustering deconvolution reveals cell phenotype shifts during the transition from healthy mucosa to fibrosis

By deconvolving spatial sequencing data with single-cell RNA-seq data from the scIBD platform, which combines highly curated single-cell datasets from CD patients and healthy controls[20] (Figure 1(D)), we further characterized the cell compartments whose phenotypes changed upon disease worsening (Figure S3(A)).

The results showed that both the deep and the superficial epithelia, enriched for crypts and postmitotic villi, respectively, had similar cell-type-specific signatures, mainly consisting of enterocyte-related gene characteristics (Figure S3(B)). However, while inflammation increased, the superficial epithelium became particularly enriched in Goblet cell-specific traits, which, in contrast, were reduced in the deep inflamed epithelium, where transit-amplifying (TA) cell-, Paneth cell-, and Tuft cell-related genes were mostly observed (Figure S3(C)–(G)). These results indicated that, in the epithelium, the deep layer underwent the most prominent change.

In the stromal compartments, including the perivascular, we observed an enrichment of signatures related to immature pericytes, stromal (1 and 2) cells, and myofibroblasts (Figure 1(E)–(H)). When inflamed, the stroma lost most of these traits while acquiring those of the transitional stroma (in the perivascular inflamed stroma), inflammatory fibroblasts (Figure 1(I) and (J)), lymphatic endothelial cells (LECs), and mesoderm (in the inflamed stroma, Figure S4(A) and (B)).

In the fibrotic compartments, we identified two distinct types of intestinal fibrosis characterized by specific molecular markers and cellular compositions. Specifically, we found a reduction of inflammatory fibroblast signatures in both the superficial and the deep fibrosis compared with the inflamed stroma, including the perivascular (Figure 1(J)). In contrast, reticular fibroblast gene signatures were increased and characterized the fibrotic compartments (Figure 1(K)), which also displayed gene signatures related to myofibroblasts (Figure 1(H)). Moreover, the superficial submucosa fibrosis showed a mesoderm-related gene signature (Figure S4(E)). Interestingly, the stromal 1- and the stromal 2-specific genes characterized the deep and the superficial fibrosis, respectively (Figure 1(H) and (G)).

The muscular compartment was characterized, as expected, by both mature and immature pericyte- (Figure S4(C) and (D)), stromal-, myofibroblast- (Figure 1(F)–(H)), and smooth muscle cell-related gene signatures (Figure S4(F)).

From this analysis, the fibrotic process emerges as an alteration of the mesenchymal compartments (stromal and muscular cells) without a significant involvement of the epithelium.

3.3. Fibrosis develops from the mesenchymal compartment

Although various studies have described fibrosis mechanistically,[21] clear molecular transitions have yet to be tracked, justifying the uncertainty around the process and the questions on the role of inflammation.

Therefore, to unravel how chronic inflammation progresses to fibrosis, we performed deconvolution of single-cell RNA-seq data[20] with the observed spatial signatures (Figure 2(A)). Uniform Manifold Approximation and Projection (UMAP) revealed the different cell populations in the single cell data (Figure 2(B)), in particular epithelial, lymphoid (CD8, CD4, ILC, plasma cells), myeloid, mesenchymal, endothelial, and neural clusters.

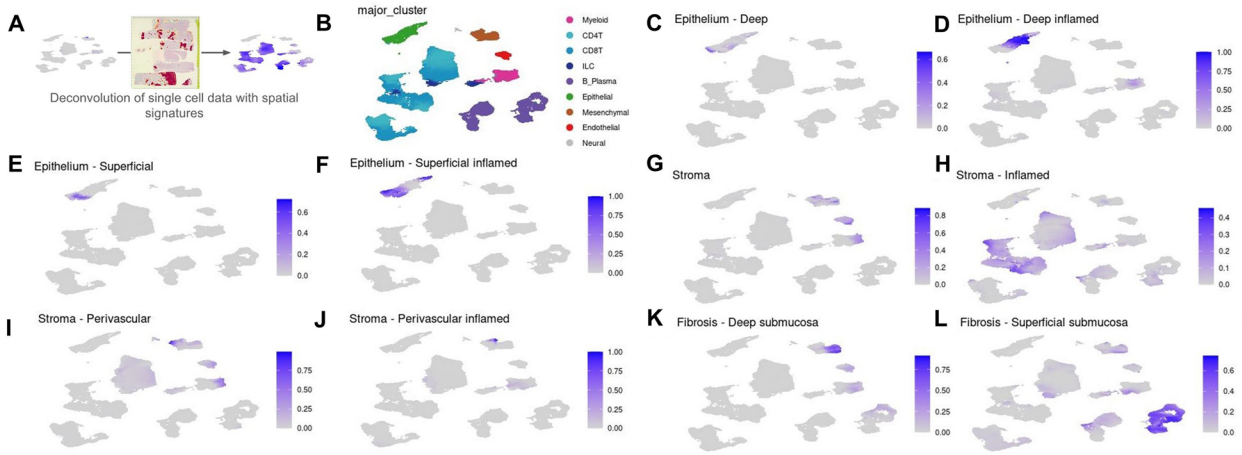

Figure 2. Fibrosis mainly develops from the mesenchymal compartment. (A) Schematic representation of single-cell data deconvolution with spatial cell signatures. (B) UMAP showing major clusters found in the scIBD dataset. (C–L) UMAP plots showing the indicated spatial signature distributions in scIBD.

First, we confirmed that our inflammation-related clusters (ie, granulation tissue and lymphoid aggregates) matched the proinflammatory single-cell data (Figure S5(A) and (B)).

Within the epithelial cluster, deconvolution with the spatial signatures revealed differences between the deep and superficial epithelia at the transcriptomic level. Notably, both changed in an inflamed environment (Figure 2(C)–(F)). As expected, the stromal compartment was part of the mesenchymal and endothelial cell clusters, also with spots in the myeloid (Figure 2(G)) consistent with the presence of resident or circulating innate immune cells physiologically overseeing stromal tissue homeostasis.[22] When inflamed, the stroma became enriched in granulation tissue and lymphoid aggregates (Figure 2(H) and Figure S5(A) and (B)). The perivascular stroma also showed mesenchymal and endothelial characteristics, with myeloid spots and no major changes upon inflammation (Figure 2(I) and (J)). These data suggest that the structural stroma underwent inflammatory activation over the disease course, while the perivascular stroma, which regulates immune cell trafficking, remained stable.

In parallel, the fibrotic compartment in the deep submucosa was mainly of mesenchymal origin with minor signals from endothelial cells and myeloid cells (Figure 2(K)), while the superficial submucosa fibrosis displayed mainly B cell signatures (Figure 2(L)). The muscular compartment, as expected, was part of the mesenchymal cell cluster (Figure S5(C)).

Together, these results confirmed that epithelial cells change their transcriptional phenotype upon inflammation but did not indicate any epithelial-to-mesenchymal transition (EMT) at this stage. On the other hand, fibrosis appears to be mainly of mesenchymal origin, with inflammatory cells highly present in the superficial submucosa.

Next, to investigate in detail the transition from mesenchymal cells to fibrosis, we performed a sub-clustering of the mesenchymal cell compartment (Figure 3(A)).

Fibrosis in the deep submucosa was mainly enriched in one cluster (Figure 3(B), cluster #1), while superficial fibrosis was characterized also by an additional cluster (Figure 3(C), clusters #1 and #2). Cluster #1 included stromal cells, both fetal and non-fetal, cycling stroma, and reticular fibroblasts, while cluster #2 was characterized by transitional stroma and mesoderm (Figure 3(D)). Based on this characterization, we thus determined that reticular fibroblasts mainly characterized the deep submucosa fibrosis, while mesodermal cells were a peculiarity of the superficial fibrosis.

Therefore, to track the transition to fibrosis in the mesenchymal compartment, we performed pseudotime analysis. In cluster #1, two starting points (start 1 and start 2) were defined, the fetal stromal and the myofibroblasts, respectively, while in cluster #2 transitional stroma was identified as the most probable beginning (start 3, Figure 3(D)–(F)). During the transition, in cluster #1 fetal stroma cells became differentiated stromal cells (end 1). At the same time, myofibroblasts underwent differentiation into reticular and inflammatory fibroblasts (end 2 and end 3) after passing through an intermediate state of cycling stroma. In cluster #2, the transitional stroma evolves to mesoderm (end 4), a transition specific to superficial submucosa-associated fibrosis.

To better characterize the cellular transition, we performed pathway analysis of the pseudotime sub-clustering to identify the biological processes (BPs) highly specific to fibrosis and most activated. Start 1 subcluster was characterized by BPs related to the negative regulation of fibroblast growth factor (FGF) and regulation of microvillus organization, the latter also activated when the transition to stroma progressed (Figure S6(A) and(B), and Figure S7(A), top panel). At the end of the transition (end 1), BPs related to cell adhesion were increased (Figure S6(C) and (D), and Figure S7(A), bottom panel). Start 2, formerly identified as myofibroblasts, activated pathways related to muscle contraction and intermediate filament assembly (Figure S6(E) and (F), and Figure S7(B), top panel). During the transition to end 2, besides activation of cell adhesion processes (Figure S3(C) and (D)), cells activated BPs related to T cell costimulation and the response to bacteria (Figure S6(G) and (H), and Figure S7(B), middle panel), while during the transition to end 3 cells mainly activated pathways related to innate immune response (Figure S6(I)–(L), and Figure S7(B), bottom panel). Finally, inflammatory pathways were highly upregulated in the transition from start 3 to end 4 (Figure S6 (K) and (L), and Figure S7(C)).

Based on these results, fibrosis evolves from the mesenchymal compartment and is constituted by stromal cells, also including inflammatory and reticular fibroblasts, the latter highly enriched in deep submucosa fibrosis. Moreover, the two types of fibrosis depend not only on the source cells but also on the

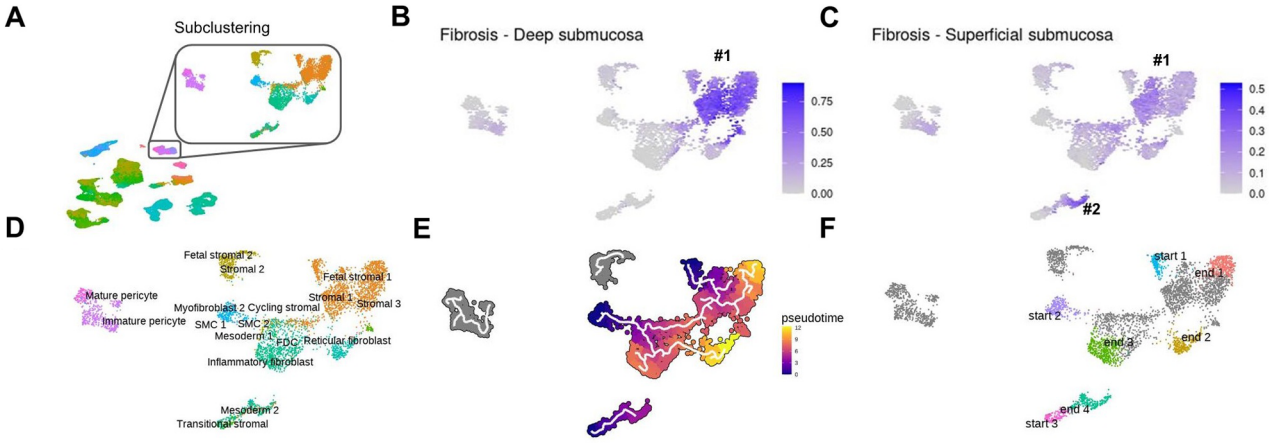

Figure 3. Pseudotime analysis of the mesenchymal compartment subclusters reveals three types of cellular transition defining fibrosis. (A) Schematic representation of mesenchymal compartment subclustering. (B–C) UMAP plots showing the deep (B) and superficial (C) submucosal fibrosis spatial signature distributions in scIBD-defined cell types. (D) UMAP showing minor clusters in scIBD mesenchymal subclustering. (E) Pseudotime analysis in the mesenchymal subclustering. (F) Seurat clustering with 200% resolution to identify pseudotime start and end clusters.

type of BPs activated. Specifically, one type is mainly characterized by cell shape changes (deep submucosa fibrosis), and the other is associated with inflammatory responses (superficial submucosa fibrosis).

3.4. Intercellular communications broaden, but weaken, as inflammation progresses to complications

Signaling crosstalk among the different compartments via ligand–receptor communications is central to tissue functioning in both physiological and pathological conditions.[23] To investigate the cell interactions and signaling network rearrangement within either the control, or L1, or L2 areas, we employed CellChat, which uses a ligand–receptor interaction database to infer, visualize, and analyze intercellular communications.[24]

In the control, most of the interactions occurred among muscle, stroma, and perivascular stroma, with an average interaction strength of around 2 (Figures S8(A) and S9(A)). Notably, the nervous system at this stage exchanged signals, with moderate strength, with the stromal and muscular compartments, indicating that, in the intestinal mucosa, the enteric nervous system also directs the correct tissue physiology by interacting with the muscle.

By contrast, intercommunication strengths changed when we performed the same analysis in the L1 and L2 areas. In L1, the interactions among muscle, stroma, perivascular stroma, and nervous system increased in number and intensity, with the highest interaction strength (between 4 and 6) with the inflamed perivascular stroma (Figures S8(B) and S9(B)). Interestingly, in L1, lymphoid aggregates began sending and receiving signals, although they were less interactive when compared to the other cell compartments. As expected, granulation tissue, characteristic of chronic inflammation, was relatively silent. Moreover, fibrotic tissues, particularly the superficial ones, mostly interacted with the inflamed perivascular stroma.

In the L1 phase, the average weight of interaction strengths was around 4, higher than in the control areas, meaning that chronic inflammation activated cell–cell interactions, mainly at the level of the inflamed perivascular stroma. This is consistent with the increased angiogenesis during inflammation, which is in charge of directing immune cell trafficking within mucosa.[25]

By proceeding to the L2 areas, almost all compartments began interacting with each other (Figures S8(C) and S9(C)), apart from the epithelium, which remained relatively "isolated." Likewise, the inflammatory areas (lymphoid and granulation tissues) were less interactive than the other stromal compartments.

While in L1 the deep submucosal fibrosis remained "silent," in L2 it became active, communicating with the other compartments more than the superficial fibrosis, in particular with the other mesenchymal compartments. Also, in L2, the inflamed perivascular stroma was the most highly activated and interactive.

Despite the overall increase in the number of interactions, within the L2 area, the average interaction strength was around 2, indicating that the peak of the intercellular communication strength was reached in L1 and that, in L2, the overall inter-signaling was reduced, although more dispersed.

3.5. Ligand–receptor analysis reveals the main actors in driving inflammation to fibrosis

To highlight the most relevant pathways among the large number of interactions observed by CellChat[16] analysis, we calculated the number of ligand–receptor signaling patterns describing the co-contribution of sent and received different pathways, for control, L1, and L2 stages (Figure S9(D)–(F)). The number of patterns was chosen to minimize the pathways featuring compartment-specific contributions and maintain sufficient co-phenetic and silhouette scores.

To track the molecular evolution of the disease, we started from the L2 stage by selecting only those pathways most specific to both the superficial and deep fibrosis, and then proceeded backward to the control stage to define the compartments possibly triggering the process. In L2, the superficial and the deep fibrosis received signaling pattern 4 (black arrow), with PECAM1 and 2 signals as the major contributors, which were sent (pattern 1) by the superficial fibrosis and, to a lesser extent, by the deep fibrosis, perivascular stroma, inflamed stroma, and the granulation tissue (Figure 4(A)). Thus, we checked for PECAM1 and 2 signaling in L1. PECAM1 (patterns 5 and 6 with a major contribution) was received by the stroma, the deep and superficial fibrosis, and the perivascular stroma, while

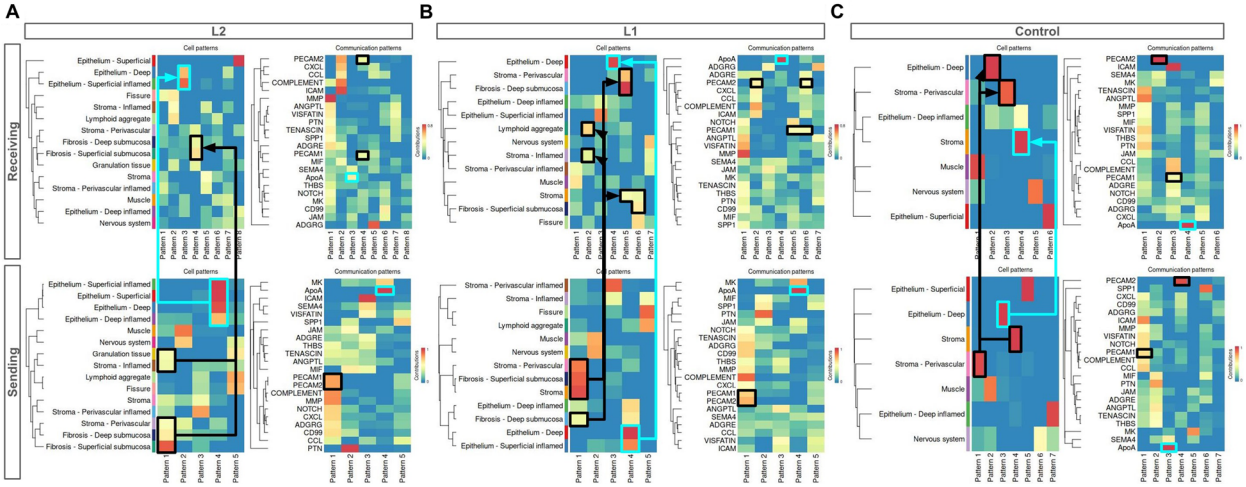

Figure 4. Ligand–receptor analysis reveals the main actors in driving inflammation to fibrosis. (A–C) Heatmaps showing receiving (top panel) and sending (bottom panel) cell and communication pattern contributions in L2 (A), L1 (B), and control (C). Black arrows and boxes indicate PECAM1/2 signaling pathways, and light blue indicates the ApoA signaling pathway.

the stroma and superficial fibrosis, lymphoid aggregates, and inflamed stroma received PECAM2 (patterns 2 and 6). Here, both PECAM 1 and 2 (pattern 1) were sent by the perivascular stroma, the stroma, the superficial, and, to a lesser extent, the deep fibrosis (Figure 4(B)).

We then calculated which compartments orchestrated this signaling in physiological conditions (control). Interestingly, PECAM1 is received and sent by the perivascular stroma (patterns 3 and 1, respectively), while PECAM2 is received (pattern 2) by the deep epithelium and sent as pattern 4 by the stroma (Figure 4(C)).

Hence, going backward from L2 to control, we identified PECAM1 and 2 as the main contributors in sustaining the fibrotic process, involving both the stromal and inflammatory compartments. In fact, in physiological conditions (control), the epithelium was involved as an additional actor in receiving PECAM2 but stopped doing so in L1. This raised the question of how the homeostasis between the stromal and the epithelial compartment is interrupted in favor of the stromal compartment only, eventually leading to activation of the fibrotic process.

We thus checked in the control which signals involved both the deep epithelium and the stroma. In the control heatmap, the deep epithelium sends ApoA (pattern 3, light blue arrow) that is received by the stroma (pattern 4, Figure 4(C)). This crosstalk weakened during disease complication, where ApoA signaling sustained, with high strength, the epithelial inflammation but not the stroma (Figure 4(A) and (B)).

From these results, we concluded that, in physiological conditions, the deep epithelium and the stroma interact via ApoA and PECAM2 signaling, while the perivascular stroma sustains itself via PECAM1 (Figure S10(A)). Upon inflammation, epithelium–stroma crosstalk decreases, and the epithelium starts fostering itself via ApoA. The stroma, along with the perivascular stroma and the fibrosis, send PECAM2-mediated signals to themselves and the lymphoid aggregates (Figure S10(B)). In the L2 stage, when chronic inflammation is established, fibrosis is self-sustained by PECAM1 and 2 signals, also sent by the granulation tissue and the stroma (Figure S10(C)). Notably, PECAM1-mediated signals continue sustaining the mesenchymal compartments across all disease stages.

3.6. ST reveals fibrosis as induced by CD38-mediated signals and their inhibition halts chronic colitis *in vivo*

Ligand–receptor analysis helped draw the molecular blueprint of CD, localizing and giving relevance to signaling pathways associated with specific compartments. By exploiting this analysis, we sought to define the molecular evolution of the disease from control to L2 by spatially mapping the ligand–receptor pairs contributing to the overall signaling.

ApoA signaling included APOA1–ABCA1 and APOA1–(CUBN+AMN) pairs. Expression of APOA1 and ABCA1 molecules was confirmed at the epithelial and stromal levels, respectively, in the control, supporting APOA1–ABCA1 pair-mediated crosstalk between the two compartments as relevant in the healthy state (Figure 5(A)). In L1 and L2 tissues, the APOA1–ABCA1 distribution was still present, but less intense and associated, particularly in the epithelial compartment, with the APOA1–(CUBN+AMN) pair (Figure 5(B) and (C)). Notably, CUBN was absent in the control, indicating that the APOA1–(CUBN+AMN) complex-mediated signaling was not involved at that stage. This expression pattern was also confirmed in single-cell data from CD samples, where APOA1$^+$ and ABCA1$^+$ cells were highly present in the epithelial and stromal clusters (Figure S11(A)–(C)), while CUBN$^+$ and AMN$^+$ cells were mainly found at the level of the epithelium (Figure S11(D) and (E)).

PECAM1 signaling included PECAM1–PECAM1 and PECAM1–CD177 interactions, the former representing the major contributor to all disease stages, at the level of the stroma (Figure 5(D)–(F)). PECAM2 signaling mainly involves PECAM1–CD38 molecules. CD38 was almost absent in the control but increased its intensity upon inflammation in the lymphoid aggregates (in L1), in the granulation tissue (in L2), and in the stromal and fibrosis compartments (Figure 5(D)–(F)). CD38 was highly present in hematopoietic cells (Figure S11(F)) but also in the mesenchymal compartment at the level of the myofibroblast-to-reticular fibroblast transition, and, to a lesser extent, in the fetal stroma-to-stroma, myofibroblast-to-inflammatory fibroblast, and transitional stroma-to-mesoderm transitions (Figure S12(A) and (B)). Notably, CD38 expression was also confirmed at the level of mesenchymal cells in the fibrotic area in an independent cohort of CD patients (Figure S12(C)).

To further support the clinical relevance of our ST data, we then correlated CD38 and APOA1 expression profiles with fibrosis development in patients by co-varying neighborhood analysis (CNA).[26] This confirmed the direct correlation between fibrosis development and disease duration adjusted for age, as widely known[27] (Figure 6(A) and (B), and Figure S12(D)). More importantly, we found opposite correlations with fibrosis for the two investigated main actors: APOA1 negatively correlated while CD38 positively correlated with fibrosis. Of note, they inversely correlated with each other (Figure 6(C)–(E)). Finally, other evidence in support of our hypothesis comes from the inflammatory bowel disease (IBD) TaMMA platform,[7] where CD38 and APOA1 are up- and down-regulated, respectively, in a larger sample of surgical specimens of ileal CD (total samples analyzed $n = 1643$, Figure S12(E) and (F)).

To demonstrate the potential for clinical translation of our findings into a therapeutic intervention that could avoid fibrosis development, we tested the inhibition of CD38 in an experimental model of chronic intestinal inflammation and fibrosis, TNBS-induced chronic colitis. The results showed that mice treated with the CD38 inhibitor in addition to TNBS do not develop chronic inflammation and colon thickening compared with the controls (Figure 6(F)–(G)), confirming the pro-inflammatory/pro-fibrotic role of CD38-mediated signaling in the intestine.

Overall, our results shed light on new mechanisms underlying CD progression and complications. We propose that APOA1–ABCA1 interaction with the stroma maintains homeostasis in the healthy tissue, exerting anti-inflammatory effects[28] on the stroma. However, during chronic inflammation, when the epithelium is compromised, APOA1–(CUBN+AMN) switches on, supporting the epithelium's survival and diverting ApoA signaling from the stroma (Figure 6(I)).

Moreover, during inflammation, immune cells, including the CD38$^+$ cells, migrate to the site of injury, and the PECAM1–CD38 interaction increases in both the stromal compartment and inflammatory sites, contributing to the transformation of the mesenchymal compartment in fibrosis (Figure 6(F)). This function is consistent with well-established role of CD38 in inflammation, including in IBD pathogenesis and fibrosis.[29–32]

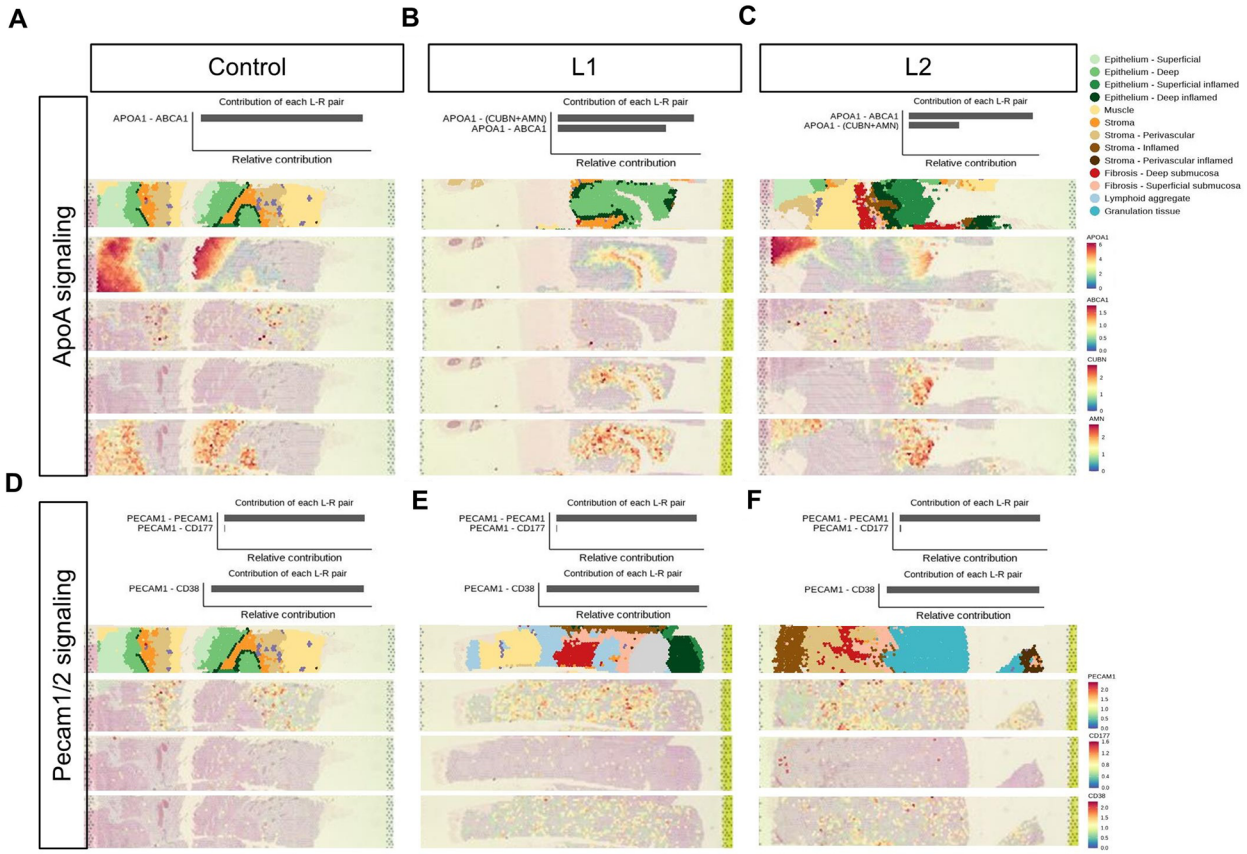

Figure 5. Ligand–receptor pair identification reveals PECAM1–CD38 interaction as the main contributor to fibrosis. (A–C) Bar graphs showing relative contribution of ligand–receptor pairs to ApoA signaling (top panel) and spatial expression pattern of the contributing genes in representative images of control (A), L1 (B), and L2 (C) spatial transcriptomics slides. (D–F) Bar graphs showing relative contribution of ligand–receptor pairs to PECAM 1 and PECAM2 signalings (top panel) and spatial expression pattern of the contributing genes in representative images of control (D), L1 (E), and L2 (F) spatial transcriptomics slides.

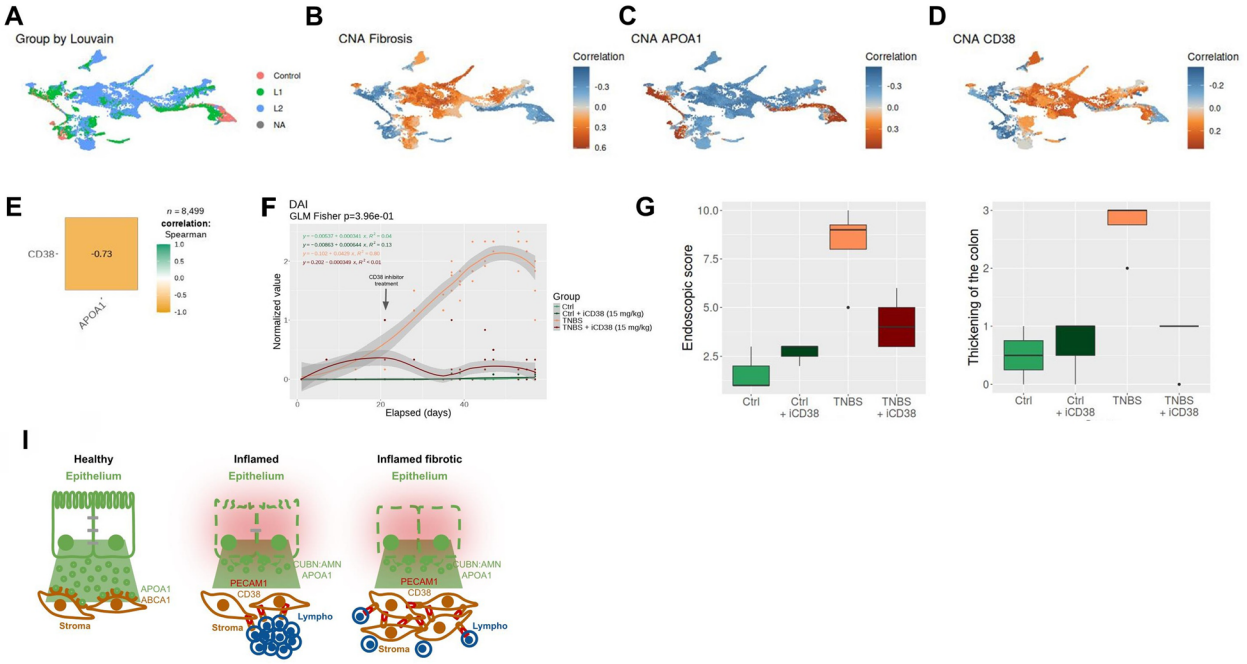

Figure 6. CD38- and ApoA1-mediated signaling contribute to fibrosis. (A) UMAP showing group distribution within spatial multidimensional scaling. (B–D) UMAPs showing fibrosis (B), APOA1 (C), and CD38 (D) expression profile correlation according to co-varying neighborhood analysis (CNA) in spatial multidimensional scaling. (E) Single-cell gene co-occurrence analysis by Spearman's correlation. (F) Disease activity index (DAI) showing colitis development over time in the indicated conditions. The black arrow indicates commencement of the CD38 inhibitor treatment. The inhibitor was administered intraperitoneally, three times a week, from the fourth week of the TNBS-induced model until mice were killed. (G) Box plots showing the endoscopic score (right panel) and thickening of the colon score (left panel) in mice in the indicated conditions. (I) Schematic representation of ApoA- and PECAM2-controlled fibrosis development.

Finally, all disease stages are supported by PECAM1 signaling to ensure the correct activity of the stromal compartment, particularly of the endothelial cells, and in mediating leukocyte trafficking within a tissue, a process known to be central in regulating intestinal inflammation.[33] Thus, PECAM1 signaling is sustained during inflammation to support tissue maintenance while simultaneously promoting fibrosis.

4. Discussion

Here we present the first spatially resolved analysis of the transition from inflammation to fibrosis in the intestine of patients with CD. Using full-thickness surgical specimens from patients with CD and healthy controls, our study confirms the cytoarchitecture rearrangements, the loss of compartment organization,[19] and the relevance of epithelial and stromal cell subtypes in the evolution of the disease to fibrosis.[34,35] In addition, the spatial resolution of our approach enabled the identification of two distinct fibrotic clusters: a superficial cluster predominantly composed of inflammatory fibroblasts and a deeper cluster enriched with reticular fibroblasts, which were uniquely associated with strictures and absent in other inflammatory settings, such as fissures and inflamed stroma. Furthermore, pseudotime analysis confirmed that reticular fibroblasts originate from activated myofibroblasts, representing the terminal differentiation stage of these cells within the fibrotic tissue.

This is in line with CD pathological traits. Indeed, inflammatory insults activate inflammatory fibroblasts to release pro-inflammatory cytokines[35,36] and coordinate the immune response. Our findings show that the superficial submucosa is highly enriched in B cells and displays activation of BPs related to the inflammatory response. At the same time, reticular fibroblasts, specialized in extracellular matrix deposition, become relevant for fibrotic tissue thickening in the deep submucosa fibrosis in the advanced disease stage.[37,38]

Notably, a recent study by Miyara and colleagues[39] applied the model of hot/cold fibrosis to cardiac injury,[40] where acute myocardial infarction (MI) leads to cold fibrosis, where only myofibroblasts are present, whereas chronic injury in heart failure leads to hot fibrosis, where, beyond myofibroblasts, macrophages are enriched. In our study, we showed the involvement of inflammatory cells (B cells, myeloid cells) in fibrotic regions in both the deep and the superficial submucosa, although B cells are most highly present, especially in the superficial submucosa (Figure 2(K) and (L)). Superficial fibrosis, with inflammatory fibroblasts and B cells, might align more closely with the "hot" fibrosis concept than deep fibrosis, primarily characterized by reticular fibroblasts and fewer inflammatory cells. This comparison highlights that while the hot/cold concept provides a useful high-level framework, the specific cellular compositions of fibrosis can vary by organ and injury context, as shown by the detailed spatial analysis in CD provided here.

In fact, our and Miyara's studies identified specific molecular interactions or cell populations as potential therapeutic targets based on their roles in driving fibrosis. In cardiac cold fibrosis, the target is the myofibroblast autocrine loop, specifically TIMP1. In our CD fibrosis model, key targets identified are PECAM2 signaling (via CD38 inhibition) and potentially restoring ApoA signaling. Comparing the targets highlights that the specific drivers of fibrosis can differ significantly depending on the organ and the nature of the injury (acute MI vs. chronic intestinal inflammation). This reinforces the idea that anti-fibrotic therapies may need to be context-specific. However, the general strategy of targeting key cell–cell communication pathways or autocrine loops, as suggested by the cardiac cell circuit model, appears to be supported by the findings in CD, where targeting CD38, involved in cell–cell interactions, shows therapeutic potential as well. In our analysis, we did not observe any indication of EMT, since epithelial cells, also when inflamed, displayed no mesenchymal-specific transcriptome characteristics. Despite previous studies describing the role of EMT in the process of fibrosis development and the large characterization at the level of specific mesenchymal markers,[41] our data did not confirm such a transition, but are in line with the latest studies at single-cell resolution, where EMT signs were not found in the epithelium, but only in the mesenchymal compartment.[8,35,42,43] Therefore, though we do not exclude that the epithelial layers we identified by ST can express single EMT-specific markers, we did not find evidence of epithelial-to-mesenchymal cell reprogramming.

Our study allowed us to track the molecular transition from control to inflamed to fibrotic. Ligand–receptor analysis, using CellChat as a useful tool for unravelling the fibrosis-related mechanisms, as previously shown elsewhere,[43–45] pointed to two main steps during disease evolution: (1) interaction signalings reached their maximum strength in the inflamed state (L1) before fibrosis development when all compartments start communicating aberrantly, probably to counteract/activate proinflammatory stimuli; and (2) the intercommunications decreased in strength but broadened in number when chronic inflammation is established and fibrosis developed (L2), probably due to cell compartment distortion, loss of well-organized crosstalk, and increase in transcriptionally inactive extracellular matrix.

Last but not least, we found that the stromal compartment coordinated the signalings in the mesenchyme even before fibrosis development, through CD38- and ApoA-mediated signaling. These two molecular switches appear to be central to the evolution of CD from inflammatory to fibrostenotic. In particular, we propose that the APOA1–ABCA1 interaction is at the basis of the immune surveillance exerted by the epithelium on the stroma, ensuring tissue homeostasis in healthy conditions. APOA1 has well-established anti-inflammatory properties. In the intestine, it characterizes a subset of epithelial cells.[46] APOA1 interaction with ABCA1 mediates anti-inflammatory effects via STAT3 activation,[28] and changes stromal cell metabolism, which, in turn, impacts immune cells.[47–49] These findings support a model where, in healthy conditions, the epithelium promotes immune surveillance through the APOA1/ABCA1 pathway.[50] However, during inflammation, APOA1 switches its interaction to the CUBN/AMN complex, crucial for epithelial cell survival in the intestine[51,52] probably as a compensatory mechanism to support the damaged epithelium, since epithelial–stromal communication is interrupted, and so is its surveillance.

Most importantly, our study identified CD38 as a driver of chronic inflammation and the fibrotic process. CD38 signaling is important for maintaining mucosal epithelial barrier homeostasis.[29,31,32] Notably, CD38 has been shown to harbor NAD^+-mediated pro-fibrotic activity via TGF-β signaling in multiple organs, supporting its profibrotic role in CD.[31,32] We believe CD38 can drive intestinal fibrosis by coordinating the reshaping of the mesenchymal compartment, as supported by our finding of CD38 expression at the transition from myofibroblasts to inflammatory and reticular fibroblasts. This is

further corroborated by our *in vivo* study, where CD38 inhibition has been noted as effective in reducing inflammation and the consequent thickening of the colon, a sign of an ongoing fibrotic process.

Moreover, we proposed ApoA signaling as a negative regulator of the transition, owing to its indirect correlation with CD38 expression and fibrosis in patients, as well as its reduced impact on the stroma during disease progression.

Our data indicate for the first time the processes underlying CD evolution to fibrotic complications at the molecular and cellular levels, pointing to specific signalings as responsible for tissue transformation.

We acknowledge that the sample size used was limited. However, by integrating our findings with previously published single-cell datasets and confirming the reproducibility of key results through different computational methods, we are confident that our conclusions robustly outline the transition from a healthy state to fibrosis from both molecular and cellular perspectives. In fact, to reinforce our work, we performed deconvolution analyses using spatial signatures on the scIBD single-cell data, a meta-analysis of 440 samples—including tissues and liquid biopsies for a total of 117 from ulcerative colitis, 51 from CD, 19 from colitis, and 253 from healthy individuals, and conversely, we deconvolved spatial data with scIBD single-cell signatures. This integrated approach, utilizing the spatial context from our limited cohort and the cellular resolution from the larger scIBD resource, significantly strengthens the biological conclusions drawn in the present study.

Nonetheless, we do not exclude the contribution of additional signaling pathways given the high heterogeneity of CD among patients.[7]

Overall, our study offers a new view on the development of intestinal fibrosis, originating from the mesenchymal compartment in the context of an inflammation-associated disruption of homeostatic mechanisms. Moreover, our findings position CD38 as a critical link in this process and a potential new target for treatment for the prevention of CD-associated fibrotic complications.

Author contributions

L.M., T.L.P., F.U.: contributed to conceptualization and writing the original draft; T.L.P., S.M., M.B., A.F., F.S., A.V., A.M., V.V., L.A., S.N., C.E.: contributed to data search and acquisition; L.M., M.R.: contributed to bioinformatics and statistical analysis; S.N., S.S.: contributed to human sample collection; M.P., V.S., A.M., V.J., L.P.B., P.S.: contributed to review and editing; S.D., F.U.: contributed to supervision; S.D., P.S., F.U.: contributed to resources and funding acquisition.

Supplementary material

Supplementary material is available at *ECCO-JCC* online.

Funding

The work was funded by the European Union—Next Generation EU—NRRP M6C2 – Investment 2.1 Enhancement and strengthening of biomedical research in the NHS under grant agreements #PNRR-MAD-2022-12375729 (CUP master C43C22001270007) to S.D. and #PNRR-MCNT2-2023-12377779 (CUP master C43C24000410007) to P.S. and F.U.; by the IoIBD Operating Grant 2024 to F.U., and by the "Ricerca Finalizzata" program by the Italian Ministry of Health under the grant agreement #RF-2021-12372637 to S.D.

Conflicts of interest

S.D. has served as a speaker, consultant, and advisory board member for Schering Plough, Abbott (AbbVie) Laboratories, Merck and Co, UCB Pharma, Ferring, Cellerix, Millenium Takeda, Nycomed, Pharmacosmos, Actelion, Alfa Wasserman, Genentech, Grunenthal, Pfizer, AstraZeneca, Novo Nordisk, Vifor, and Johnson and Johnson. L.P.-B. has served as consultant for Merck, AbbVie, Janssen, Genentech, Ferring, Tillots, Vifor, Pharmacosmos, Celltrion, Takeda, Biogaran, Boerhinger-Ingelheim, Lilly, Pfizer, Jndex Pharmaceuticals, Amgen, Sandoz, Celgene, Biogen, Samsung Bioepis, Alma, Sterna, Nestlé, Enterome, Mylan, HAC- Pharma, and Tigenix, and has served as speaker for Merck, AbbVie, Janssen, Genentech, Ferring, Tillots, Vifor, Pharmacosmos, Celltrion, Takeda, Boerhinger-Ingelheim, Pfizer, Amgen, Biogen, and Samsung Bioepis. V.J. has received has received consulting/advisory board fees from AbbVie, Alimentiv Inc (formerly Robarts Clinical Trials), Arena Pharmaceuticals, Asahi Kasei Pharma, Asieris, Bristol Myers Squibb, Celltrion, Eli Lilly, Ferring, Flagship Pioneering, Fresenius Kabi, Galapagos, GlaxoSmithKline, Genentech, Gilead, Janssen, Merck, Mylan, Pandion, Pendopharm, Pfizer, Protagonist, Reistone Biopharma, Roche, Sandoz, Second Genome, Takeda, Teva, Topivert, and Vividion; speaker's fees from AbbVie, Ferring, Galapagos, Janssen Pfizer Shire, Takeda, and Fresenius Kabi. The other authors declare no conflicts of interest.

Data availability

Data from spatial transcriptomics are available at the NCBI GEO repository with accession number GSE277348 (https://www.ncbi.nlm.nih.gov/geo/query/acc.cgi?acc=GSE277348).

References

1. Torres J, Mehandru S, Colombel J-F, Peyrin-Biroulet L. Crohn's disease. *Lancet*. 2017;389:1741-1755. https://doi.org/10.1016/S0140-6736(16)31711-1
2. Lichtenstein GR, Loftus EV, Isaacs KL, Regueiro MD, Gerson LB, Sands BE. ACG clinical guideline: management of Crohn's disease in adults. *Am J Gastroenterol*. 2018;113:481-517. https://doi.org/10.1038/ajg.2018.27
3. Rieder F, Kessler S, Sans M, Fiocchi C. Animal models of intestinal fibrosis: new tools for the understanding of pathogenesis and therapy of human disease. *Am J Physiol Gastrointest Liver Physiol*. 2012;303:G786-801. https://doi.org/10.1152/ajpgi.00059.2012
4. Mandlik JS, Patil AS, Singh S. Next-Generation Sequencing (NGS): platforms and applications. *J Pharm Bioallied Sci*. 2024;16:S41-S45. https://doi.org/10.4103/jpbs.jpbs_838_23
5. Seyed Tabib NS, Madgwick M, Sudhakar P, Verstockt B, Korcsmaros T, Vermeire S. Big data in IBD: big progress for clinical practice. *Gut*. 2020;69:1520-1532. https://doi.org/10.1136/gutjnl-2019-320065
6. Corridoni D, Chapman T, Antanaviciute A, Satsangi J, Simmons A. Inflammatory bowel disease through the lens of single-cell RNA-seq technologies. *Inflamm Bowel Dis*. 2020;26:1658-1668. https://doi.org/10.1093/ibd/izaa089

7. Massimino L, Lamparelli LA, Houshyar Y, et al. The Inflammatory Bowel Disease Transcriptome and Metatranscriptome Meta-Analysis (IBD TaMMA) framework. *Nat Comput Sci*. 2021;1:511-515. https://doi.org/10.1038/s43588-021-00114-y
8. Ke B-J, Abdurahiman S, Biscu F, et al. Intercellular interaction between FAP+ fibroblasts and CD150+ inflammatory monocytes mediates fibro-stenosis in Crohn's disease. *J Clin Invest*. 2024;134: https://doi.org/10.1172/JCI173835
9. Zhang C, Wang L, Shi Q. Computational modeling for deciphering tissue microenvironment heterogeneity from spatially resolved transcriptomics. *Comput Struct Biotechnol J*. 2024;23:2109-2115. https://doi.org/10.1016/j.csbj.2024.05.028
10. Satija R, Farrell JA, Gennert D, Schier AF, Regev A. Spatial reconstruction of single-cell gene expression data. *Nat Biotechnol*. 2015;33:495-502. https://doi.org/10.1038/nbt.3192
11. Korsunsky I, Millard N, Fan J, et al. Fast, sensitive and accurate integration of single-cell data with Harmony. *Nat Methods*. 2019;16:1289-1296. https://doi.org/10.1038/s41592-019-0619-0
12. Kueckelhaus J, Frerich S, Kada-Benotmane J, et al. Inferring histology-associated gene expression gradients in spatial transcriptomic studies. *Nat Commun*. 2024;15:7280. https://doi.org/10.1038/s41467-024-50904-x
13. Pham D, Tan X, Balderson B, et al. Robust mapping of spatiotemporal trajectories and cell–cell interactions in healthy and diseased tissues. *Nat Commun*. 2023;14:7739. https://doi.org/10.1038/s41467-023-43120-6
14. Cao J, Spielmann M, Qiu X, et al. The single-cell transcriptional landscape of mammalian organogenesis. *Nature*. 2019;566:496-502. https://doi.org/10.1038/s41586-019-0969-x
15. Liang Q, Huang Y, He S, Chen K. Pathway centric analysis for single-cell RNA-seq and spatial transcriptomics data with GSDensity. *Nat Commun*. 2023;14:8416. https://doi.org/10.1038/s41467-023-44206-x
16. Jin S, Plikus MV, Nie Q. CellChat for systematic analysis of cell–cell communication from single-cell and spatially resolved transcriptomics. *Nat Protoc*. 2025;20:180-219. https://doi.org/10.1038/s41596-024-01045-4
17. Massimino L, Palmieri O, Facoetti A, et al. Gut virome-colonising Orthohepadnavirus genus is associated with ulcerative colitis pathogenesis and induces intestinal inflammation in vivo. *Gut*. 2023;72:1838-1847. https://doi.org/10.1136/gutjnl-2022-328375
18. Dolinger M, Torres J, Vermeire S. Crohn's disease. *Lancet*. 2024;403:1177-1191. https://doi.org/10.1016/S0140-6736(23)02586-2
19. Li C, Kuemmerle JF. Mechanisms that mediate the development of fibrosis in patients with Crohn's disease. *Inflamm Bowel Dis*. 2014;20:1250-1258. https://doi.org/10.1097/MIB.0000000000000043
20. Nie H, Lin P, Zhang Y, et al. Single-cell meta-analysis of inflammatory bowel disease with scIBD. *Nat Comput Sci*. 2023;3:522-531. https://doi.org/10.1038/s43588-023-00464-9
21. D'Alessio S, Ungaro F, Noviello D, Lovisa S, Peyrin-Biroulet L, Danese S. Revisiting fibrosis in inflammatory bowel disease: the gut thickens. *Nat Rev Gastroenterol Hepatol*. 2022;19:169-184. https://doi.org/10.1038/s41575-021-00543-0
22. Roozendaal R, Mebius RE. Stromal cell-immune cell interactions. *Annu Rev Immunol*. 2011;29:23-43. https://doi.org/10.1146/annurev-immunol-031210-101357
23. Valls PO, Esposito A. Signalling dynamics, cell decisions, and homeostatic control in health and disease. *Curr Opin Cell Biol*. 2022;75:102066. https://doi.org/10.1016/j.ceb.2022.01.011
24. Jin S, Guerrero-Juarez CF, Zhang L, et al. Inference and analysis of cell–cell communication using CellChat. *Nat Commun*. 2021;12:1088. https://doi.org/10.1038/s41467-021-21246-9
25. Jeong J-H, Ojha U, Lee YM. Pathological angiogenesis and inflammation in tissues. *Arch Pharm Res*. 2021;44:1-15. https://doi.org/10.1007/s12272-020-01287-2
26. Reshef YA, Rumker L, Kang JB, et al. Co-varying neighborhood analysis identifies cell populations associated with phenotypes of interest from single-cell transcriptomics. *Nat Biotechnol*. 2022;40:355-363. https://doi.org/10.1038/s41587-021-01066-4
27. Pariente B, Cosnes J, Danese S, et al. Development of the Crohn's disease digestive damage score, the Lémann score. *Inflamm Bowel Dis*. 2011;17:1415-1422. https://doi.org/10.1002/ibd.21506
28. Tang C, Liu Y, Kessler PS, Vaughan AM, Oram JF. The macrophage cholesterol exporter ABCA1 functions as an anti-inflammatory receptor. *J Biol Chem*. 2009;284:32336-32343. https://doi.org/10.1074/jbc.M109.047472
29. Schneider M, Schumacher V, Lischke T, et al. CD38 is expressed on inflammatory cells of the intestine and promotes intestinal inflammation. *PLoS ONE*. 2015;10:e0126007. https://doi.org/10.1371/journal.pone.0126007
30. Piedra-Quintero ZL, Wilson Z, Nava P, Guerau-de-Arellano M. CD38: an immunomodulatory molecule in inflammation and autoimmunity. *Front Immunol*. 2020;11:597959. https://doi.org/10.3389/fimmu.2020.597959
31. Shi B, Wang W, Korman B, et al. Targeting CD38-dependent NAD+ metabolism to mitigate multiple organ fibrosis. *IScience*. 2021;24:101902. https://doi.org/10.1016/j.isci.2020.101902
32. Shi B, Amin A, Dalvi P, et al. Heavy-chain antibody targeting of CD38 NAD+ hydrolase ectoenzyme to prevent fibrosis in multiple organs. *Sci Rep*. 2023;13:22085. https://doi.org/10.1038/s41598-023-49450-1
33. Woodfin A, Voisin M-B, Nourshargh S. PECAM-1: a multi-functional molecule in inflammation and vascular biology. *Arterioscler Thromb Vasc Biol*. 2007;27:2514-2523. https://doi.org/10.1161/ATVBAHA.107.151456
34. Kong L, Pokatayev V, Lefkovith A, et al. The landscape of immune dysregulation in Crohn's disease revealed through single-cell transcriptomic profiling in the ileum and colon. *Immunity*. 2023;56:444-458.e5. https://doi.org/10.1016/j.immuni.2023.01.002
35. Li J, Simmons AJ, Hawkins CV, et al. Identification and multimodal characterization of a specialized epithelial cell type associated with Crohn's disease. *Nat Commun*. 2024;15:7204. https://doi.org/10.1038/s41467-024-51580-7
36. Wei K, Nguyen HN, Brenner MB. Fibroblast pathology in inflammatory diseases. *J Clin Invest*. 2021;131. https://doi.org/10.1172/JCI149538
37. Griffin MF, desJardins-Park HE, Mascharak S, Borrelli MR, Longaker MT. Understanding the impact of fibroblast heterogeneity on skin fibrosis. *Dis Model Mech*. 2020;13. https://doi.org/10.1242/dmm.044164
38. Gomes RN, Manuel F, Nascimento DS. The bright side of fibroblasts: molecular signature and regenerative cues in major organs. *Npj Regen Med*. 2021;6:43. https://doi.org/10.1038/s41536-021-00153-z
39. Miyara S, Adler M, Umansky KB, et al. Cold and hot fibrosis define clinically distinct cardiac pathologies. *Cell Syst*. 2025;16:101198. https://doi.org/10.1016/j.cels.2025.101198
40. Adler M, Mayo A, Zhou X, et al. Principles of cell circuits for tissue repair and fibrosis. *IScience*. 2020;23:100841. https://doi.org/10.1016/j.isci.2020.100841
41. Jiang H, Shen J, Ran Z. Epithelial–mesenchymal transition in Crohn's disease. *Mucosal Immunol*. 2018;11:294-303. https://doi.org/10.1038/mi.2017.107
42. Zhang Y, Wang J, Sun H, et al. TWIST1+FAP+ fibroblasts in the pathogenesis of intestinal fibrosis in Crohn's disease. *J Clin Invest*. 2024;134: https://doi.org/10.1172/JCI179472

43. Mukherjee PK, Nguyen QT, Li J, et al. Stricturing Crohn's disease single-cell RNA sequencing reveals fibroblast heterogeneity and intercellular interactions. *Gastroenterology*. 2023;165:1180-1196. https://doi.org/10.1053/j.gastro.2023.07.014
44. Dovrolis N, Valatas V, Drygiannakis I, et al. Landscape of interactions between stromal and myeloid cells in ileal Crohn's disease; indications of an important role for fibroblast-derived CCL-2. *Biomedicines*. 2024;12:1674. https://doi.org/10.3390/biomedicines12081674
45. Thottakara T, Padmanabhan A, Tanriverdi T, et al. Single-nucleus RNA/ATAC-seq in early-stage HCM models predicts SWI/SNF-activation in mutant-myocytes, and allele-specific differences in fibroblasts. *BioRxiv*. 2024. https://doi.org/10.1101/2024.04.24.589078
46. Li J, Simmons AJ, Chiron S, et al. A specialized epithelial cell type regulating mucosal immunity and driving human Crohn's disease. *BioRxiv*. 2023. https://doi.org/10.1101/2023.09.30.560293
47. Zhao G-J, Yin K, Fu Y-C, Tang C-K. The interaction of ApoA-I and ABCA1 triggers signal transduction pathways to mediate efflux of cellular lipids. *Mol Med*. 2012;18:149-158. https://doi.org/10.2119/molmed.2011.00183
48. Zhu Y, Li X, Wang L, Hong X, Yang J. Metabolic reprogramming and crosstalk of cancer-related fibroblasts and immune cells in the tumor microenvironment. *Front Endocrinol (Lausanne)*. 2022;13:988295. https://doi.org/10.3389/fendo.2022.988295
49. Salminen A, Kaarniranta K, Kauppinen A. Tissue fibroblasts are versatile immune regulators: An evaluation of their impact on the aging process. *Ageing Res Rev*. 2024;97:102296. https://doi.org/10.1016/j.arr.2024.102296
50. Rosenblum D, Naik S. Epithelial-immune crosstalk in health and disease. *Curr Opin Genet Dev*. 2022;74:101910. https://doi.org/10.1016/j.gde.2022.101910
51. Ge Y, Zadeh M, Mohamadzadeh M. Vitamin B12 regulates the transcriptional, metabolic, and epigenetic programing in human ileal epithelial cells. *Nutrients*. 2022;14:2825. https://doi.org/10.3390/nu14142825
52. Kozyraki R, Fyfe J, Kristiansen M, et al. The intrinsic factor-vitamin B12 receptor, cubilin, is a high-affinity apolipoprotein A-I receptor facilitating endocytosis of high-density lipoprotein. *Nat Med*. 1999;5:656-661. https://doi.org/10.1038/9504